Protein Structure and Folding:

Active Glutaminase C self-assembles into a supra-tetrameric oligomer which can be disrupted by an allosteric inhibitor.

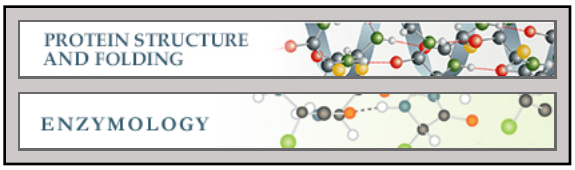

Amanda Petrina Scota Ferreira, Alexandre Cassago, Kaliandra Almeida Goncalves, Marilia Meira Dias, Douglas Adamoski, Carolline Fernanda Rodrigues Ascencao, Rodrigo Vargas Honorato, Juliana Ferreira de Oliveira, Igor Monteze Ferreira, Camila Fornezari, Jefferson Bettini, Paulo Sergio Lopes Oliveira, Adriana Franco Paes Leme, Rodrigo Villares Portugal, Andre Luis Berteli Ambrosio and Sandra Martha Gomes Dias

J. Biol. Chem. *published online August 8, 2013*

Access the most updated version of this article at doi: 10.1074/jbc.M113.501346

Find articles, minireviews, Reflections and Classics on similar topics on the JBC Affinity Sites.

Alerts:

- When this article is cited
- When a correction for this article is posted

Click here to choose from all of JBC's e-mail alerts

This article cites 0 references, 0 of which can be accessed free at
http://www.jbc.org/content/early/2013/08/08/jbc.M113.501346.full.html#ref-list-1

Downloaded from http://www.jbc.org/ at FAPESP - Brazil Consortia on August 12, 2013

JBC Papers in Press. Published on August 8, 2013 as Manuscript M113.501346
The latest version is at http://www.jbc.org/cgi/doi/10.1074/jbc.M113.501346

Active Glutaminase C self-assembles into a supra-tetrameric oligomer which can be disrupted by an allosteric inhibitor*

Amanda Petrina Scotá Ferreira[1,†], Alexandre Cassago[2,†], Kaliandra de Almeida Gonçalves[1,†], Marília Meira Dias[1], Douglas Adamoski[1], Carolline Fernanda Rodrigues Ascenção[1], Rodrigo Vargas Honorato[1], Juliana Ferreira de Oliveira[1], Igor Monteze Ferreira[1], Camila Fornezari[1], Jefferson Bettini[2], Paulo Sérgio Lopes Oliveira[1], Adriana Franco Paes Leme[1], Rodrigo Villares Portugal[2], Andre Luis Berteli Ambrosio[1,#] and Sandra Martha Gomes Dias[1,#]

Laboratórios Nacionais de [1]Biociências e [2]Nanotecnologia, Centro Nacional de Pesquisa em Energia e Materiais, Campinas-SP 13083-100, Brazil.

*****Running title: The supra-tetrameric oligomerization-dependent GAC activation.

[†] APSF, AC and KAG contributed equally to this work.
[#] ALBA and SMGD contributed equally to this work.

To whom correspondence may be addressed: Andre LB Ambrosio or Sandra MG Dias, Laboratório Nacional de Biociências - LNBio, CNPEM, Rua Giuseppe Máximo Scolfaro, 10.000, Pólo II de Alta Tecnologia, Campinas, SP, 13083-100, Brazil. Tel: +55 19 3512 1115/Fax: +55 19 3512 1004; E-mail: andre.ambrosio@lnbio.cnpem.br and sandra.dias@lnbio.cnpem.br.

Keywords: Glutamine metabolism; Cancer; Warburg effect

Background: GAC supplies for increased metabolic needs of tumors because of exclusive localization and kinetic properties.

Results: Assembly of higher-than-tetramer oligomers is mandatory for enzyme activation *in vitro* and in cellular assays. Bis-2-(5-phenylacetamido-1,3,4-thiadiazol-2-yl)ethyl sulfide disrupts the oligomers.

Conclusion: Novel molecular mechanism for GAC activation is proposed.

Significance: The data impacts on the development of therapies targeting GAC in tumors, with emphasis on allosteric inhibitors.

ABSTRACT

The phosphate-dependent transition between enzimatically inert dimers into catalytically-capable tetramers has long been the accepted mechanism for the glutaminase activation. Here, we demonstrate that activated Glutaminase C (GAC) self-assembles into a helical, fiber-like double-stranded oligomer and propose a molecular model, consisting of seven tetramer copies per turn per strand interacting via the N-terminal domains. The loop L_{321}RFNKL_{326} is projected as the major regulating element for self-assembly and enzyme activation. Furthermore, the previously identified *in vivo* lysine acetylation (Lys311 in humans, Lys316 in mouse) is here proposed as an important down-regulator of super-oligomer assembly and protein activation. BPTES (Bis-2-(5-phenylacetamido-1,3,4-thiadiazol-2-yl)ethyl sulfide), a known glutaminase inhibitor, completely disrupted the higher-order oligomer, explaining its allosteric mechanism of inhibition via tetramer-stabilization. A direct correlation between the tendency to self-assemble and the activity levels of the three mammalian glutaminase isozymes was established, with GAC being the more active enzyme while forming the longest structures. Lastly, the ectopic expression of a fiber-prone super-active GAC mutant in MDA-MB 231 cancer cells provided considerable proliferative advantages to transformed cells. These findings yield unique implications for the development of GAC-oriented therapeutics targeting tumor metabolism.

Cancer cells have a well-established dependence on glutamine metabolism to support their highly proliferative status. Apart from acting as a source for nitrogen as well as reductive

Downloaded from http://www.jbc.org/ at FAPESP - Brazil Consortia on August 12, 2013
Copyright 2013 by The American Society for Biochemistry and Molecular Biology, Inc.

power, its anabolic carbon skeletons can be siphoned from the TCA cycle to be used as building blocks for the growing and dividing cells (1, 2). Both Myc and Rho GTPases have been shown to stimulate Glutaminase C (GAC), an isozyme that possesses a distinct cellular localization as well as activation levels purported to provide the aforesaid proliferative advantage to cancer cells (3-5).

We have recently described the structural determinants of the phosphate-dependent activation mechanism of GAC, based on the tetramerization-induced lifting of a so-called gating loop (L_{321}RFNKL_{326}; NCBI sequence NP_001106854.1), which controls substrate accessibility to the active site. We showed that phosphate binds inside the catalytic pocket, resulting in allosteric stabilization of tetramers and facilitating substrate entry by outcompeting with the product, glutamate, to guarantee enzyme cycling (5). Additionally, recent publications have provided structural insights into glutaminase inhibition by making use of the small molecules BPTES and 968 (6-9). Nevertheless, the precise descriptions of their modes of inhibition are still lacking.

Renewed interest in cancer metabolism has prompted an innovative warfront against metabolic enzymes, aiming at the development of alternative and efficient therapeutic opportunities. Glutaminase is a key target in this sense (2, 4, 10, 11) and the need for new and accurate biochemical and structural information, in order to speed up and improve the development of successful therapies, is therefore essential. In this regard, we now provide novel information demonstrating that the assembly of higher-order, fiber-like GAC oligomers, henceforth termed the GAC superstructure, is necessary for proper enzyme activation both *in vitro* and in a cancer cell model. First, we demonstrate that the superstructure is mandatorily present when GAC is in the active form, as shown by negatively stained samples analyzed by Transmission Electron Microscopy (TEM). The tendency towards the superstructure correlates well with the activation levels induced by phosphate among GAC and the other twomammalian glutaminase isozymes, the Kidney-type Glutaminase (KGA) and the Liver-type Glutaminase (LGA). While LGA is a synonym for the GLS2 glutaminase, KGA and its splicing variant GAC are both usually indistinguishably referred to as GLS1. Moreover, we observe that the addition of the GLS1 inhibitor BPTES hampers protein polymerization by stabilizing inactive tetramers.

Further research identified a subset of key residues involved in the superstructure-formation process. These are located in the gating loop, as well as at the N- and C-termini, which have been previously shown to be key structural features for enzyme activation (5, 12). One specific gating loop mutant, GAC.K325A, both assembles into the superstructure and shows a 600-fold enhancement in catalytic efficiency towards L-glutamine, even in the absence of phosphate. Conversely, GAC.R322A, also at the gating loop, abrogated protein activation and impeded superstructure formation. A previously identified *in vivo* post-translational modification of human GLS1 (13), the acetylation of Lys316 (equivalent to Lys311 in human), was also studied in this context. We show that the acetylation mimetic GAC.K316Q does not assemble into higher-order oligomers and this modification likely inhibits protein activity in cells. By combining data from point-mutants, TEM, mass spectrometry (MS) and computational biology, we offer a low-resolution model for the superstructure assembly. The superstructure is based on a double-stranded helix containing tetramers interacting with each other via the N-terminus domain. Lastly, we demonstrate that MDA-MB 231 cells silenced for the endogenous GAC expression and stably expressing an ectopic fiber-prone super-active mutant, proliferates more, consume higher amounts of glutamine and grow bigger than the wild-type and mock-transformed cells. Our results shed new light on the molecular mechanism of phosphate-dependent activation of the glutaminases and highlight the importance of the development of allosteric inhibitors when targeting GAC in tumors.

EXPERIMENTAL PROCEDURES

Protein production, enzymatic assay, size-exclusion serial dilution and site-directed mutagenesis. – Recombinant protein expression and purification, the streamlined glutaminase activity assay, as well as the size-exclusion analysis of serial dilutions, were performed as previously published (5). Point mutants were

Downloaded from http://www.jbc.org/ at FAPESP - Brazil Consortia on August 12, 2013

generated with the QuikChange II Site-Directed Mutagenesis kit (Stratagene) following fabricant instructions. The inhibition assays using BPTES (kindly provided by Dr. Chi Van Dang, Abramson Cancer Center) were done with GAC or GAC.K325A at 5 nM and BPTES diluted in DMSO, the last always at a 0.5% final concentration. Measurements were done in triplicates and analyzed using GraphPad Prism 5.00 (GraphPad Software) and Origin 8.1 (OriginLab). The parameters of the dose-response curve were determined by fitting error bar-weighted logistic function, in the form of y = A2 + (A1-A2)/(1 + (x/x0)^p), where A1 is the initial apparent turnover rate (absence of inhibitor), A2 is the turnover rate at saturating concentrations of inhibitor, x0 is the half-maximum inhibitory concentration, or IC_{50}, and p is the Hill slope.

Transmission Electron Microscopy – For visualization of negatively stained grids, protein samples, at a concentration ranging from 0.5 to 1 μM, were deposited onto glow-discharged holey carbon-coated grids for 60 seconds followed by two steps of blotting and staining with 2% uranyl acetate. Images were acquired between -1 and -3 μm defocus at 15,000x to 80,000x magnification using a Jeol JEM-2100 operating at 200 kV and recorded on a F-416 CMOS camera (TVIPS, Germany).

Crystallization and X-ray crystallography – Crystallization experiments were performed at 291 K using the conventional sitting drop vapor diffusion technique. Drops were made by mixing three parts of protein (at 3.3 mg/ml) to one of well solution, containing 17% PEG 3350, 0.2 M NaCl and 0.1 M Bis-TRIS pH 6.5. Clusters of plates were observed after 5 days and used as seeds for a standard streak-seeding in a mother-liquor solution containing 11% PEG 3350, 0.2 M NaCl and 0.1 M Bis-TRIS pH 6.5. Before data collection at cryogenic temperature (100 K), harvested crystals were cryoprotected with 10% ethylene glycol added to the mother liquor. X-ray diffraction data was obtained at the D03B-MX1 beamline at LNLS, Brazil. Data was processed using Mosflm (14) and Scala (15). The first set of phases was obtained by the molecular replacement as implemented in Phaser (16), using the dataset from the ligand-free form of GAC, available under PDB code 3ss3 (5). Positional and B-factor refinement cycles were carried out with Phenix (17). Manual building of the extra portions and real space refinement, including Fourier electron density map inspection, were performed with Coot (18). The overall stereochemical quality of the final models and the agreements between them and experimental data were assessed by the program Molprobit (19) and the appropriate Coot routines.

Cross-linking analysis of GAC complexes by LC-MS/MS – GAC complexes were reduced (5 mM *dithiothreitol*, 25 min at 56°C), alkylated (14 mM iodoacetamide, 30 min at room temperature in the dark), and digested with trypsin (Promega). The samples were lyophilized in a vacuum concentrator and reconstituted in 0.1% formic acid. Four and a half micrograms of the resulting peptide was analyzed on an LTQ Velos Orbitrap mass spectrometer (Thermo Fisher Scientific) coupled with LC-MS/MS by an EASY-nLC system (Thermo Fisher Scientific) through a Proxeon nanoelectrospray ion source. Peptides were separated by a 2-90% acetonitrile gradient in 0.1% formic acid using a pre-column EASY-Column (2 cm x ID100 μm, 5 μm particle size) and an analytical column PicoFrit Column (20 cm x ID75 μm, 5 μm particle size, New Objective) at a flow rate of 300 nL/min over 65 min. The nanoelectrospray voltage was set to 2.2 kV and the source temperature was 275°C. The instrument methods in LTQ Velos Orbitrap were set up in the data dependent acquisition mode of HCD fragmentation. The full scan MS spectra (m/z 300–1,600) were acquired in the Orbitrap analyzer after accumulation to a target value of $1xe^6$. The resolution in the Orbitrap system was set to r=60,000 and the 5 most intense peptide ions with charge states ≥ 2 were sequentially isolated to a target value of 50,000 and fragmented in HCD with normalized collision energy of 40% with the resolution in the Orbitrap system was set to r=7,500 for MS/MS. The signal threshold for triggering an MS/MS event was set to 80,000 counts and activation time of 0.1 ms was used. Dynamic exclusion was enabled with exclusion size list of 400 and exclusion duration of 60 s, and repeat count of 2. For cross-linking analysis, the raw data files generated by Xcalibur v.2.1 (Thermo Fisher Scientific) were converted to a peak list format (mgf) using Proteome Discoverer version 1.3 (Thermo Fisher Scientific). The mgf files were analyzed in MassMatrix software (www.massmatrix.net) to automatically search

Downloaded from http://www.jbc.org/ at FAPESP - Brazil Consortia on August 12, 2013

chemical cross-linkage against database containing the GAC amino acid sequences. The parameters for cross-linking analysis were carbamidomethylation (+57.021460 Da) as fixed modification, oxidation of methionine (+15.99491 Da) as variable modifications, chemical cross-linked with disuccinimidyl suberate-DSS (138.06808 Da) non-cleavable by enzymes, four trypsin missed cleavages and a tolerance of 10 ppm for precursor and 0.02 Da for fragment ions (20). Potential cross-linked peptides were manually validated. This experiment was independently performed four times for the tetramer form and seven times for the super-oligomer form. Unique lysine linkages (underlined in the following peptides) were only observed in the tetramer samples, between residues Lys181 and Lys207 (α-KCVQSNIVLLTQAFR AND β-LKECMDMLR), Lys202 and Lys578 (α-LTLQTTSDGVMLDKDLFK AND β-DTVWKK) and Lys403 and Lys512 (α-SGVAGGILLVVPNVMGMMCWSPPLDKMGN SVK AND β-EKK)..

Computational biology – To obtain a model of the glutaminase fiber we applied a previously developed rigid-body docking algorithm restrained by experimental DSS cross-linking data (20). Initially, we reconstructed both the N- and C-terminal regions of the monomers using a loop reconstruction routine and placed a copy of the tetramer, namely the ligand domain, on the N-terminal of the receptor domain. Using only the exclusive inter-monomer linkage that were observed in our reconstructed model (Lys181-Lys207) we selected the decoy that was in the lowest energy range and within 11 Å of lysine pair distance.

Cell assays – MDA-MB 231 cells were purchased from ATCC (initial passage of 29) and cultivated in RPMI 1640 medium (Cultilab, Campinas, Brazil) supplemented with 10% fetal bovine serum (Cultilab, Campinas, Brazil). The pcDNA3.1/V5-His-hGAC (GAC-V5) clone was kindly provided by Dr. Richard Cerione (Cornell University, Ithaca, NY, USA), and the mutation K320A (equivalent to K325A in the mouse gene) performed with the QuikChange II Site-Directed Mutagenesis Kit (GAC.K325A-V5), following the fabricant instructions. Lipofectamine transfected cells were G418 selected for stable expression, which was confirmed by western blotting. The Mock control was obtained by transfecting cells with empty vector. To accomplish the endogenous GAC knock down, the same cell clones were transduced with lentiviral particles containing pLKO-shGAC plasmid (For: 5'-CCGGCCTCTGTTCTGTCAGAGTTCTCGAGA ACTCTGACAGAACAGAGGTTTTTG-3' and Rev: 5'-AATTCAAAAACCTCTGTTCTGTCAGAGTTC TCGAGAACTCTGACAGAACAGAGG-3') and pool of cells were selected for puromicin resistance. Cells were lysed with 20 mM Tris-HCl pH 7.5, 150 mM NaCl, 1% Triton X-100, 1 mM EDTA, 1 mM DTT, 1 mM $NaVO_4$, 1 mM β-glycerol phosphate, 11 $\mu g.mL^{-1}$ aprotinin, 11 $\mu g.mL^{-}1$ pepstatin and 1 mM PMSF. The lysates were resolved by SDS-PAGE, and the proteins transferred to polyvinylidene fluoride membranes. The membranes were incubated overnight with the primary antibodies diluted in 20 mM Tris, 135 mM NaCl and 0.1% Tween 20. The primary antibodies were detected with horseradish peroxidase-conjugated secondary antibodies followed by exposure to Pierce SuperSignal West Pico Substrate. We used anti-V5 1:10000 (Life Technologies), anti-GAC custom made by Genescript as previously described in (5) at 1 $\mu g.mL^{-1}$, anti-Vinculin 1:1000 (Cell Signaling) and anti-VDAC 1:1000 (Cell Signaling). As for the immunofluorescence and glutamine consumption studies, MDA-MB 231 cells were seeded in a 6 wells plate (Becton Dickson) at a density of $2,5x10^{-5}$ $cels.cm^{-2}$, cultivated for 48 hours at 37 °C with 5% of CO2 and then fixated and permeabilized with 3.7% Formaldehyde in PBS/0.2% Triton X-100. Cells were blocked with 3% BSA in PBS/0.8% Triton X-100, and incubated at room temperature for 1 hour, with anti-V5 1:20000 diluted in 3% BSA in PBS/0.8% Triton X-100. Goat secondary anti mouse-Alexa633 (Life Technologies), diluted in blocking solution (1:200) was used to reveal ectopically expressed V5-tagged GAC. Nuclei and actin were stained with 2.5 $\mu g.mL^{-1}$ DAPI (Sigma) and Phalloidin-Alexa488 (1:40), respectively. Data were collected with the plate-reader Fluorescence Microscope Operetta (Perkin Elmer) and cell number and area quantified using the software Harmony 3.0. Glutamine consumption from the culture media was assessed using the Bio-Profile Basic 4 (Nova Biomedical). BPTES-treated cells were allowed to attach for 24 hours and then had

Downloaded from http://www.jbc.org/ at FAPESP - Brazil Consortia on August 12, 2013

the media replaced by fresh media added of 10 μM of the inhibitor for 48 hours. For the whole cell lysate glutaminase activity assay, cells were lysed by ressuspension in 25 mM Hepes pH 8.0, 150 mM NaCl, 1 mM EDTA, 0.01% Triton X-100 and 1x Protease Inhibition Solution (Qiagen) followed by 20 strokes through an insulin needle. Glutaminase activity assay of the whole-cell extracts was performed following the published streamlined assay (5), using 5 μg of lysate per well and L-glutamine concentration of 7.5 mM. Diameter of detached viable cells was measured by the Countess (Invitrogen) after tripsinization and Trypan blue incubation.

In cell protein cross-linking – Approximately $3x10^6$ cells were seeded in 10 cm plates and allowed to adhere overnight. On the next day, the media was removed and cells washed twice with PBS and incubated for 24 hours with 2 mM L-photo-leucine and 4 mM L-photo-methionine (Pierce) in leucine- and methionine-free DMEM supplemented with 10% PBS-dialyzed FBS. After this incubation, the media was removed, cells washed twice with PBS and then irradiated at 365 nm for 15 minutes in the Epi Chemi II Darkroom equipment (UVP Laboratory Products). Cells were harvested for lysis and cross-linked proteins were resolved by 3-15% Step Gradiente SDS-PAGE (3%, 9% and 15% SDS-PAGE solutions prepared with 50:1 Acrylamide:Bisacrylamide mix, poured one after another in volume proportions of 1,5:2:1.). The immunoblotting was performed with the anti-V5 1:10000 (Life Technologies) as described in the preceding section.

Estimation of intracellular glutamine concentration in breast tumor cells – From metabolomics experiments on tumor samples, Yuneva and colleagues (21) reported a relationship of 40 to hundreds nanomoles of glutamine for each gram of protein. We have found that unattached GAC.K325A-V5, GAC-V5 and mock transformed MA-MDB 231 cells, have an average diameter of 13.3, 10.9 and 10.6 μm, respectively. Assuming a spherical shape for these cells, the following cell volume can be calculated: 1.2 nL (GAC.K325A-V5 cells) and 0.6 nL (GAC-V5 and mock cells). From these cells, we have quantified using the Pierce BCA Protein Assay Kit (ThermoScientific), on average, 0.233 grams of protein for $2x10^6$ cells. Based on the lowest detected glutamine amount from Yuneva and colleagues (21) of 40 nmoles Gln/g protein, we estimate that these cells contained between 3.7 to 7.4 mM glutamine.

Quantitative PCR – RNA samples were extracted using the kit RNAeasy Mini (Qiagen) following the fabricant instructions. cDNA synthesis and PCR amplification were performed with the kits SuperScript III First-Strand Synthesis System for RT-PCR (Invitrogen) and Power SYBR Green PCR Master Mix (Applied Biosystems), respectively, as instructed by the fabricants. Samples were run on the Applied Biosystems 7500 Real-Time PCR System and analyzed following the $2^{-\Delta\Delta CT}$ method. Primers used: (i) Both endogenous and ectopic GAC – For: 5´-GATCAAAGGCATTCCTTTGG-3´ and Rev: 5´-TACTACAGTTGTAGAGATGTCC-3´ ; (ii) Ectopic GAC only – For: 5´-AGAATGGAAAGTCTGGGAGAGAAA-3´ and Rev: 5´-CCGAGGAGAGGGTTAGGGATA-3´; (iii) SN2 – For: 5´-GGCTTGGTAGTGTTTGCCAT-3´ and Rev: 5'-GGGCAAAGAGTAAACCCACA-3; (iv) ASCT2 – For: 5'-ATGAAACACTTGGGCTAC-3' and Rev: 5'-ATGACCGAAACAAGGAAA-3'; (v) rRNA 18S – For: 5'-ATTCCG ATAACGAACGAGAC-3' and Rev: 5'-TCACAGACCTGTTATTGCTC-3'.

RESULTS

Active GAC forms a rod-like supra-tetrameric structure – We have previously documented that wild-type GAC, when in the presence of its activator inorganic phosphate (Pi), showed a tendency to form molecular species larger than tetramers, and that this behavior was counteracted when the concentration of NaCl, a known glutaminase inhibitor, was increased in the protein solution (5, 12). Although the structural nature of the higher-order species remained elusive at that time, it was curious to note that there was a significantly major shift towards higher-than-tetramer oligomers in the case of the activity-enhancer mutation Phe327Ser (GAC.F327S, Fig. 1A, top right box).

In the course of further studies of mammalian glutaminase's molecular mechanism of activation, we used TEM to better understand the self-assembly process. Firstly, recombinant GAC (in the absence of Pi) was used to set up

Downloaded from http://www.jbc.org/ at FAPESP - Brazil Consortia on August 12, 2013

negatively stained grids. Image analysis, after sampling around 100 randomly chosen particles, allowed the determination of two perpendicular size distributions (exemplified in Fig. 1B): a short dimension, with a mean size of 7 ± 1 nm, and a longer one of 8 ± 1 nm (Fig. 1C, upper box), both close to those expected for the dimer particle (5). In contrast, particles formed in the presence of 20 mM phosphate had a larger and more heterogeneous size distribution on the grid. Whereas the shorter dimension doubled on average (18 ± 3 nm), there was clearly favored growth across the long dimension, averaging 88 ± 31 nm (Fig. 1C, lower box). The box chart with scatter plot for the size survey is shown in Fig. 1D.

The equilibrium between the GAC oligomeric species depends on protein concentration, phosphate and NaCl (5). To circumvent the dissociative effects of protein dilution and work at appropriate protein concentrations for TEM characterization, superstructure assembly was stabilized by adding the cross-linking agent DSS (disuccinimidyl suberate), in the presence of 20 mM phosphate, and then purified by gel-filtration. Under the conditions used, the superstructures eluted in the void volume of the column. The appropriate DSS concentration and time of incubation was previously established by a dose-response assay (data not shown). The negative-stained micrographs showed evidence for the formation of elongated, chain-like, non-branched filaments, heterogeneous in length which favored side-on adsorption to the carbon film (Fig. 1E). Some of the observed particles, such as those in Fig. 1C top right and middle boxes, seem to resemble side-by-side aggregation of simpler filaments (left and bottom boxes).

We have previously identified the gating loop as essential for the phosphate-dependent activation process of the GLS1 isoforms (5). By replacing residues in the gating loop by alanine, we identified a point-mutation (GAC.K325A) which conferred a 670-fold increase in catalytic efficiency over that found for the wild-type enzyme, even in the absence of inorganic phosphate (GAC.K325A $k_{cat\text{-}app}$ /$K_{m\text{-}app}$ of 281.8 $mM^{-1}.s^{-1}$ compared with 0.42 $mM^{-1}.s^{-1}$ for GAC) (Fig. 1F). Both negative staining TEM (Fig. 1G, left box) and size-exclusion chromatography (Fig. 1A, bottom left box) confirmed a much greater particle size distribution for this mutant, even in non-crosslinked samples. For example, TEM analysis showed dimensions of 17 ± 2 nm and 107 ± 79 nm, for the short and long dimensions, respectively, in the absence of phosphate (Fig. 1D). More importantly, this mutant assembles into oligomers visually similar to the ones formed with the wild type protein (Fig. 1C, rightmost boxes), guaranteeing that the mutation is only enhancing the oligomerization capability. The K325A mutation uncouples the protein dependence on phosphate for activation and further confirms the positive correlation between the superstructure assembly and enzyme activation. On the other hand, a second point mutation within the gating loop, affecting Arg322 (termed GAC.R322A), was enough to generate a catalytically inactive mutant irresponsive to phosphate ($k_{cat\text{-}app}$ /$K_{m\text{-}app}$ of 0.6 $mM^{-1}.s^{-1}$ at 20 mM Pi against 3.6 $mM^{-1}.s^{-1}$ for the wild-type) which, accordingly, did not assemble into super-oligomers (Fig. 1F and 1G, right box). The dimensions observed for particles of GAC.R322A in the presence of 20 mM Pi were very similar to those for the wild-type protein in the absence of Pi (7 ± 1 nm and 8 ± 2 nm, for the short and long dimensions, respectively) (Fig. 1D).

Superstructure among glutaminase isozymes – GAC is the most active of the three known mammalian glutaminase isozymes in response to inorganic phosphate (5). In order to further investigate the correlation between increased activity and larger oligomeric species, we observed the ability of Kidney-type Glutaminase (KGA) and Liver-type Glutaminase (LGA or GLS2) to assemble into supra-tetrameric structures by TEM. Superstructure assembly was induced at 20 mM phosphate, stabilized by cross-linking with DSS and subsequently gel-filtration purified. A tendency towards longer oligomers correlates well with the activity levels of the three isozymes. More specifically, GAC – the most active glutaminase at 20 mM Pi – forms the longest rod-shape oligomers (Fig. 2, top left box), followed by KGA (Fig. 2, top right box), and then LGA (Fig. 2, bottom left box), which has been previously shown to be enzymatically insensitive to Pi (5, 22) and to not form the superstructure. The mean values for the shortest and longest dimensions of the particles are 16 ± 2 nm and 181 ± 108 nm for GAC, 14 ± 3 nm and 74 ± 26 nm for KGA and 9 ±

Downloaded from http://www.jbc.org/ at FAPESP - Brazil Consortia on August 12, 2013

2 nm and 12 ± 3 nm for LGA (Fig. 2, bottom right box).

BPTES disrupts GAC superstructure – Counter intuitive to the current dimer-to-tetramer model of activation for GLS1, the inhibitor BPTES has been shown to lock GLS1 into an inactive yet tetrameric form (6). Interested in deciphering the mode of inhibition by which BPTES exerts its effect and its relationship with the formation of the superstructure, we determined a detailed BPTES dose-response curve for GAC in the presence of 20 mM Pi. This phosphate concentration was chosen as it is closer to the physiological one under hypoxic conditions (23), and substantially stimulates GAC catalytic activity (5). We observed a strong inhibitory effect on GAC, where nanomolar levels of BPTES affected the maximum catalysis rate, $k_{cat\text{-}app}$, without changing the $K_{m\text{-}app}$ for glutamine (Fig. 3A), a clear indication of an allosteric non-competitive inhibitor as already published by others (6, 7). Curiously, beyond 200 nM BPTES, a secondary effect is observed and the inhibitor started affecting also the $K_{m\text{-}app}$ (a three-fold increase compared to the absence of BPTES), re-defining BPTES as a mixed-mode inhibitor (Fig. 3A). By fitting an error bar-weighted logarithimic function to explain the decrease in the turnover rates of the enzyme due to the increased presence of inhibitor, we obtained an IC_{50} of 80.4 ± 7.2 nM for BPTES, which is consistent with the value provided by DeLaBarre and colleagues (7). Upper and lower limits for the catalytic rates are 16.4 and 7.9 s^{-1}, respectively, with a Hill slope of 1.7 ± 0.2 (R^2 = 0.99), indicating cooperative binding (Fig. 3A). Concerning the effect on $K_{m\text{-}app}$, upper and lower limits are 4.6 and 13.8 mM, with an IC_{50} of 629 ± 61 nM for BPTES (Hill slope of 2.0 ± 0.3, R^2 = 0.99).

Concomitant with the studies above, we have also determined the crystal structure of mouse GAC in complex with BPTES (2.77 Å resolution, R_{factor} of 25.3% and R_{free} of 29.5%, Table 1). Although similar to previously reported BPTES-bound glutaminase structures, with two inhibitor molecules tightly accommodated at the tetramer interface, and an average backbone r.m.s.d. of 0.44 and 0.56 Å when superposed to PDB structures 3UO9 and 3VOZ, respectively (7, 8), our crystal form presents a key unique feature. As a consequence of the binding of the small molecule to the tetramer interface, the main chain of the gating loop – consistently poorly ordered across all the GAC crystallographic models – is in a stable open conformation in all four monomers. This is due especially to the contacts made mainly between BPTES and Lys325, and consequently the loop assumes the conformation of a one-turn helix (Fig. 3B and 3C). Fifteen hydrogen bonds are made between a dimer of GAC and one BPTES molecule (data not shown). Eleven residues from each monomer share the interface with BPTES, occluding a combined total area of 620 $Å^2$. Eighty percent of the total solvent-accessible surface of BPTES (788 $Å^2$) is buried upon interaction with the enzyme.

Next, we assessed the effects of BPTES on the formation of GAC super-oligomers. TEM and size-exclusion chromatography of wild-type GAC samples prepared in the presence of phosphate and the inhibitor and subsequently cross-linked, showed that regardless of whether BPTES is added prior or after protein incubation in 20 mM phosphate, complete disruption of the superstructure is observed at a concentration of 30 μM of BPTES (Fig. 3D). The distribution of the disrupted particles on the grids is similar to the wild-type protein in the absence of phosphate and BPTES, as shown in Fig. 1A, top.

Finally, we observed that the mutant GAC.K325A, besides being hyper-active, is also catalytically insensitive to BPTES as determined by a dose-response curve (Fig. 3E). Accordingly, BPTES is incapable of disrupting non-crosslinked GAC.K325A oligomers, assembled in the presence or absence of phosphate (Fig. 3F).

Superstructure characterization – Due to its heterogeneous length distribution, the GAC superstructure is intrinsically inappropriate for crystallization. However, by combining TEM, chemical cross-linking followed by MS analysis, and computational biology, we provide a low-resolution model for the superstructure. The extended particles tend to adsorb to the microscopy grids in a very limited number of orientations. However, the best micrographs show a combination of translational and rotational symmetry elements lying parallel to the polymer, thus yielding a helical symmetry along its longitudinal axis. Detailed analysis of low-pass filtered images provided its geometrical attributes. The observed spiral polymer, under particular

Downloaded from http://www.jbc.org/ at FAPESP - Brazil Consortia on August 12, 2013

staining conditions, resembles a right-handed double-stranded helix, with a rise per turn of about 53 ± 2 nm, a strand inclination of 25° and an average width for a single strand of 6.6 ± 0.7 nm (Fig. 4A).

Simultaneously, size exclusion-purified crosslinked polymers – as well as GAC crosslinked in the tetrameric form (used as a control) – were digested with trypsin and the resulting peptides subjected to liquid chromatography coupled to tandem mass spectrometry. The cross-linked peptides were modeled based on the crystal structure of the tetramer, using a spacer arm length for DSS of about 11.4 Å as a restraint for maximum distance between the side chain amine groups of linked lysines. This was necessary in order to distinguish between the different possible inter- and intra-molecular cross-links. Unique linkages were only observed in the tetramer samples (spectra shown in Fig. 4B), between residues Lys181 and Lys207 (both located in the outer N-terminal portion of the same monomer), Lys202 and Lys578 (the latter located at the C-terminus) and Lys403 and Lys512 (both within the glutaminase domains, flanking the active site of two different monomers) as depicted in Fig. 4C. The observation that these DSS-mediated links are unable to form upon polymerization suggests occlusion of their respective surfaces from the solvent when in the superstructure form. One lysine residue from each of the cross-linked pairs was then substituted by an oppositely-charged glutamate residue and the individually mutated proteins (termed GAC.K202E, GAC.K207E and GAC.K512E) were tested for super-oligomer-dependent glutaminase activity. Both N-terminal mutants, GAC.K202E and GAC.K207E, resulted in enzymes with enhanced activity (Fig. 4D, left box), which coherently formed bigger particles, when compared to wild-type GAC (Fig. 4D, right box). Conversely, the glutaminase domain mutant GAC.K512E fully lost the phosphate-dependent enzymatic capability and, accordingly, the ability to self-assemble into the super-oligomers. The three point mutations reinforce the need for super-oligomer formation for protein enzymatic activity and, most importantly, further show the importance of regions unrelated to and distant from the catalytic pocket for super-oligomer formation and enzyme activation. Moreover, it evidences that mutations beyond the catalytic site and the glutaminase domain are capable of affecting protein oligomerization and activity.

In the original biochemical characterizations of recombinant GLS1, Kenny and co-workers demonstrated the importance of the GLS1 N-terminal portion for enzyme activity by generating a truncated, catalytically inactive, recombinant construct (12). Nevertheless, subsequent crystal structures of GAC clearly showed no direct participation of residues belonging to the N-terminal portion in catalysis or even their requirement for the proper folding or stabilization of the active site. Based on the dimensions observed in the GAC crystal structures, the average width of 66 Å for a single strand indicates that polymerization occurs along the longest axis of the tetramer, thus suggesting an end-to-end interaction via N-terminal regions. The growth is thus consistently favored in one direction and may occur indefinitely, since N-terminal sticky ends will always be available at both termini (computational docking of several tetramers simulating strand growth is shown in Fig. 4C, left illustration). Therefore, since activity is dependent on filament assembly and the N-terminal portion is key for such, we provide a plausible explanation for the findings of Kenny and co-workers (12).

Next, in order to generate a model for the double-stranded filamentous structure, the coordinate files of two single strands were manually coiled around each other, using the helical parameters as restraints (Fig. 4E). The Gaussian low-pass filter applied to the reference micrographs remove spatial frequencies higher than 0.028 $Å^{-1}$, thus resulting in an estimated 35 Å resolution in real space. According to its overall dimensions, both length-wise and angle-wise, the estimated minimum repeating unit (one full helical turn) is composed of seven tetramers in each of the entwined strands. The intrinsic two-fold dihedral symmetry of the tetramer (5) renders it unnecessary to determine whether the double-stranded helix is of a parallel or anti-parallel nature since each strand is apolar. To validate the model against the experimental data, an F_{calc} Fourier electron density map was generated by the program FFT (24) (to 35 Å maximum resolution), using structure factors calculated from the three-dimensional double-stranded coordinate file, and

Downloaded from http://www.jbc.org/ at FAPESP - Brazil Consortia on August 12, 2013

subsequently theoretically projected in two-dimensions, using the electron microscopy software Imagic (25). The end result is shown in the right panel of Fig. 4E and presents features which are fully comparable to those observed in the representative micrographs of Fig. 1E, bottom box, especially concerning the presence of an alternating pattern of narrow, compact regions of high density interspersed with broad, disc-like regions of low density.

Lastly, Lys311 in human GLS1 glutaminases was found to be a target for *in vivo* acetylation by high-resolution mass spectrometry analysis (13). This lysine residue belongs to the glutaminase domain and is located on the opposite surface in relation to the catalytic pocket and the gating loop, with no direct participation in the active site. In order to evaluate the effects of this reversible, post-translational modification over superstructure formation and therefore protein activation, we have generated a point mutant in the equivalent residue of the mouse protein (GAC.K316Q) replacing it by a glutamine residue, so as to mimic the non-charged nature of acetylated lysine. Interestingly, the newly mutated protein was characterized as less sensitive to the activator phosphate with the concomitant lowered tendency to assemble into the super-oligomers, keeping the protein in sizes compatible to only tetramers and dimers (Fig. 4D, left and right boxes).

GAC super-structure in cell model – To further demonstrate the importance of the super-structure assembly for GAC enzymatic activation, we generated stable clones of the MDA-MB 231 breast cancer cell line expressing either the human V5-tagged wild-type or the GAC.K325A mutant proteins, as well as cells transformed with a mock plasmid. Although in humans the appropriate numbering should be GAC.K320A (NCBI reference sequence AAD47056.1), we have decided to keep GAC.K325A (mouse GAC) for the sake of coherence throughout the paper. Cell clones were selected to present comparable levels of ectopic V5-tagged mRNA and protein, while not presenting abnormally higher levels of ectopic expression (Fig. 5A and 5B). Proper mitochondrial localization of the ectopic protein was confirmed by cell fractionation and immunoblotting (data not shown). Two distinct phenotypes were readily observed for the GAC.K325A-V5 cells, when compared to the GAC-V5 and mock counterparts. Firstly, GAC.K325A-V5 cells were, on average, much larger and heterogeneous in size, as based on the measurement of cell area (Fig. 5C). More specifically, while the GAC-V5 and the mock transformed cells presented similar, normally distributed cell areas, peaking at 593 and 600 μm^2 respectively, the GAC.K325A-V5 population was much more heterogeneous in size (relative standard deviation of 89%) and still about 7% larger, averaging 637 μm^2. Secondly, the mutant-transformed cells proliferated about 10% more than the wild-type and mock-transfected cells, as determined by the quantification of cell numbers (Fig. 5D). The average diameter of unattached (trypsinized) cells was also assessed in order to account for the effects of cell spreading on the area measurements. GAC.K325A-V5 cells presented the largest diameters, averaging at 13.3 μm (n=178), when compared to the wild type GAC–V5 (10.9 μm, n=151) and mock cells (10.6 μm, n=174) (data not shown).

Next, glutamine uptake from the culture media was evaluated after 48 hours of plating. We found that whereas the glutamine consumption levels for the GAC and the mock-transformed cells was deemed indistinguishable (0.78 ± 0.09 and 0.81 ± 0.07 nmol/L per cell, respectively), GAC.K325A-V5 cells consumed 40% more glutamine (1.16 ± 0.07 nmol/L per cell), as shown in Fig. 5E. In parallel, we showed that GAC.K325-V5 cells do not express more of the glutamine transporters ASCT2 and SN2 (Fig. 5F). To account for the observed increase in glutamine consumption, we assessed the glutaminase activity levels in a physiological level of L-glutamine (7.5mM) and observed that the reaction rates for the GAC.K325A-V5 cells are 40 to 50% higher when compared to the other two clones (Fig. 5G). Faster turnover rates were also consistently observed for the recombinant mutant protein, as show in the first section.

To inspect for higher-than-tetramer oligomer formation within the living cells, cells were grown in the presence of photo-reactive amino acids and then exposed to UV light (at 365 nm), followed by immunoblotting against the whole-cell extract. The data clearly showed that GAC.K325A-V5 was crosslinked *in cell* into higher molecular weight species than GAC-V5 (Fig. 5H). Although the cross-linked species did

Downloaded from http://www.jbc.org/ at FAPESP - Brazil Consortia on August 12, 2013

not extend as far as those observed for the recombinant protein *in vitro* – likely due to the hetero-oligomerization between the V5-tagged mutant protein and endogenous wild-type GAC inside the mitochondria – the differential cross-linking pattern is evident. We have shown that the enzymatic activity of the recombinant mutant GAC.K325A is unaffected by BPTES treatment (Fig. 3E), which, accordingly, did not disrupt the superstructure (Fig. 3F). As a further confirmation that the super-oligomer formation is important for the observed phenotypes, we treated cells with 10 μM of BPTES. As expected, GAC.K325A-V5 cells still grew more and consumed higher amounts of glutamine than BPTES-treated control cells (Fig. 5I). BPTES treatment has drastically decreased the glutamine consumption on all the cell clones because it likely disrupted hetero-oligomers (formed by endogenous wild-type GAC and ectopic GAC.K325A-V5) and because it is also inhibits KGA (6). Despite, the ectopic expression of GAC.K325A was able to improve the proliferation and growth phenotype of the cells.

Lastly, to exclude the possibility that the difference in cell proliferation and growth, as well as Gln uptake for the GAC.K325A-V5 cells were due to higher amounts of endogenous enzyme (in comparison to control cells), as well as to highlight the ectopic protein activity, we knocked down endogenous GAC by using a shRNA target to its mRNA 3`UTR (Fig. 5B). Not surprisingly, the previously observed phenotypic differences became enhanced. The mutant-transformed cells grew 30% more and were 40% bigger, while consuming about 2.2 times more glutamine per cell, than the wild-type-expressing cells (Fig. 5J). Accordingly, the activity levels assessed from the whole cell extract, in the presence of 7.5 mM L-glutamine, were 75% higher than the control assays (Fig. 5J). Overall, this collection of results directly demonstrated that the phenotypic differences above resulted from the presence of an ectopically-expressed, hyper-active and higher-molecular-weight prone protein GAC.K325-V5, which presented the same biochemical features and the intrinsic tendency to assemble into a superstructure as the recombinant mutant protein.

DISCUSSION

Previous biochemical studies have established that GLS1 glutaminases are mainly found as inactive dimers and that the presence of phosphate correlates with changes leading to tetramerization and enzyme activation (26, 27). We provide here novel information in that regard, and show that the catalytic activation of the GLS1 glutaminases is directly linked to a fiber-like supra-tetrameric assembly, which correlates well with activation levels of the three glutaminase isozymes. The first observations of this phenomenon were provided around forty years ago, using purified glutaminase from pig renal extract (28, 29). The formation of extended polymers was later used to purify the native enzyme by size-exclusion, allowing its first biochemical and kinetic characterization (30), thus implying that our results are not an artifact of recombinantly-expressed, truncated protein constructions, or even the chemically induced intermolecular cross-linking. Robinson and colleagues have also documented larger oligomers for recombinant GLS1 in the presence of phosphate (6). The right-handed double-stranded molecular model that we propose here, when two-dimensionally projected using electron microscopy software, is not only in fully agreement with our experimental micrographs but also with the phosphate-borate induced form and the shadow-casting reported by Olsen and colleagues in 1973 (29). Some of our micrographs suggest lateral association between two polymers, as seen, for instance in Fig. 1E (top right and middle boxes), and 2 (top left box), as well as those of the GAC.K325A mutant (Figs. 1E and 3F). Regardless of these side-by-side associations, only the longitudinal growth seems to be connected to an increase in protein activity. Such a feature was also observed by Olsen and coworkers (29). Furthermore, it is also worth mentioning that with regard to the glutaminolytic pathway, polymerization is not exclusive to GLS1 glutaminases. Glutamic Dehydrogenase (GDH) from bovine liver has been shown to self-assemble into long multi-chain tubular structures under appropriate conditions (31). It is plausible then, that non-pathogenic polymer assembly may be a widespread process for the functioning of other metabolic enzymes.

Robinson and collaborators first demonstrated biochemically that BPTES inhibits

Downloaded from http://www.jbc.org/ at FAPESP - Brazil Consortia on August 12, 2013

the GLS1 isoform (but not the liver-type isozyme, LGA/GLS2) by interfering with its phosphate-dependent allosteric activation and promoting the stabilization of the glutaminase into an inactive tetrameric form, later confirmed structurally (6-8). Our collection of results indicates that BPTES inhibits GAC by trapping the gating loop at a rigid open conformation, which in turn prevents super-oligomer formation. Although the tetramer- and phosphate-induced opening of this loop is necessary for enzyme activity, its intrinsic flexibility seems to play a major role on the enzymatic process. Indeed, we verified by molecular dynamics simulation on the tetramer that, while phosphate binding to the catalytic site increases the gating loop flexibility, both L-glutamate (enzyme inhibition by L-glutamate has been reported for the kidney isoform of GLS1 (32)) and the presence of BPTES freezes the gating loop into a less mobile state (data not shown).

We observed from the kinetic studies with the GAC.K325A mutant that filament formation results in a drastic decrease in the Michaelis constant of the protein, over 100 fold, compared to the wild-type enzyme, in the absence of the activator Pi. A much greater accessibility of the active site to the substrate is suggested upon polymerization, as well as a key role of the gating loop in this process, a phenomenon which is fully reversed when Arg322 is replaced by alanine. Therefore, the present work unveils a new role for the gating loop, which besides regulating substrate accessibility to active site, also controls the reversible protein polymerization. Due to experimental limitations, which led to a low-resolution 35 Å model, we are unable to describe the specific interactions that hold both the single and the double strands together and result in a fully activated enzyme. However, based on the most diverse effects generated mainly by the individual point mutations, it is plausible to suggest that shape complementarity is the driving force for self-assembly, and can only be fully achieved after specific surface charges are enhanced or neutralized, an outcome only attainable in the presence of a polyanion such as the phosphate ion. This is especially true in the case of the gating loop, where the replacement of two closely positioned, long and positively charged residues (Arg322 and Lys325) by alanine, had antagonic effects with regards to protein self-assembly and activation. Concomitantly, major torsions in the relative positions of the monomers inside the tetramer – which are still experimentally undetected, since all GAC crystal structures available to date are virtually identical – may be required for gating loop-mediated super-oligomer formation. The binding of BPTES, which shares an extensive area and a large number of hydrogen bonds at the tetramer interface as well as holds the loop into a rigid conformation (besides reducing the flexibility of the tetramer) would also prevent the gating loop from making these contacts. Such torsions in the tetramer cannot be predicted from our manually built model, but could possibly be described in the future from higher resolution experimental data, such as by cryo-electron microscopy.

Recently, Katt and colleagues described a potential binding site for the GAC inhibitor 968 (9). In the proposed model, the small molecule docks inside a concave surface region formed at the dimerization interface of two GAC glutaminase domains. The 968 binding region lies very close to the N-terminal portion of GAC, which is predicted here to be involved in the polymerization of the enzyme. The authors further showed that 968 is unable to bind and inhibit a previously phosphate-activated enzyme, which is in full consistency with what we present. Once GAC oligomers are assembled, due to the occlusion of the putative 968 binding site and the possible conformational changes in the N-terminal portion of the enzyme required for self-assembly, they cannot be reversed by the addition of 968, explaining its limited inhibitory capacity on an already activated enzyme. However, if 968 is bound to free tetramers, than such conformational changes cannot be subsequently achieved, stopping GAC activation via self-assembly. Given the complementary modes of inhibition for BPTES and 968, acting at different stages of enzyme assembly and polymerization, one might envision that a synergy in inhibition would result when both are administered to glutaminase sensitive transformed cell. To our knowledge, this still needs testing.

Our findings also suggest a role for the previously detected *in vivo* acetylation of Lys311 in human GLS1 glutaminases (13). We propose that this post-translational modification down-

Downloaded from http://www.jbc.org/ at FAPESP - Brazil Consortia on August 12, 2013

regulates the enzymatic levels by antagonizing the formation of the active super-oligomers. Given that acetylation is a reversible post-translational modification, it is plausible to suppose that glutaminase super activation may, at least in part, be regulated by acetyltransferases and deacetylases, yet to be identified.

Finally, we need to state that we would not expect that micrometer-long GAC polymers to assemble inside the mitochondria. Rather, a more tangible scenario might be the presence of shorter, heterogeneous filaments, similar to those observed in Fig. 1A, lower box. Nonetheless, direct visualization of such in the mitochondria has proven a difficult task. We showed that the intrinsically bound to self-assemble, super active mutant GAC.K325A, was capable of providing growth and proliferation advantages to cells. However, a more important conclusion that can be drawn from these experiments is that an increased level of GAC in the mitochondria by itself is not sufficient to increase cell proliferation. The protein must be in the active form for such a phenotype to become evident. In cells, phosphate accumulation induced by hypoxia, for instance (23, 33), or even post-translational modifications, such as phosphorylation, could trigger polymerization, suggesting the possibility of distinct therapeutic opportunities for 968-like and BPTES-like inhibitors. Overall, our results reinforce the importance in focusing on the development of allosteric over active site-targeted inhibitors, glutamine-analogue inhibitors, when targeting GAC in tumors. This would result in preferred isoform specific inhibitors, since LGA (GLS2), necessary for glutamine metabolism in the liver and brain, does not assemble into super-oligomers, as well as avoiding the undesirable cross-inhibition of amidotransferases (21).

REFERENCES

1. Gaglio, D., Metallo, C.M., Gameiro, P.A., Hiller, K., Danna, L.S., Balestrieri, C., Alberghina, L., Stephanopoulos, G., and Chiaradonna, F. (2011) Oncogenic K-Ras decouples glucose and glutamine metabolism to support cancer cell growth. *Mol. Syst. Biol.* **7**, 523

2. Le, A., Lane, A.N., Hamaker, M., Bose, S., Gouw, A., Barbi, J., Tsukamoto, T., Rojas, C.J., Slusher, B.S., Zhang, H., Zimmerman, L.J., Liebler, D.C., Slebos, R.J., Lorkiewicz, P.K., Higashi, R.M., Fan, T.W., and Dang, C.V. (2012) Glucose-independent glutamine metabolism via TCA cycling for proliferation and survival in B cells. *Cell Metab.* **15**, 110–121

3. Gao, P., Tchernyshyov, I., Chang, T.C., Lee, Y.S., Kita, K., Ochi, T., Zeller, K.I., De Marzo, A.M., Van Eyk, J.E., Mendell, J.T., and Dang CV. (2009) c-Myc suppression of miR-23a/b enhances mitochondrial glutaminase expression and glutamine metabolism. *Nature* **458**, 762–765

4. Wang, J.B., Erickson, J.W., Fuji, R., Ramachandran, S., Gao, P., Dinavahi, R., Wilson, K.F., Ambrosio, A.L., Dias, S.M., Dang, C.V., and Cerione, R.A. (2010) Targeting mitochondrial glutaminase activity inhibits oncogenic transformation. *Cancer Cell* **18**, 207–219

5. Cassago, A., Ferreira, A.P., Ferreira, I.M., Fornezari, C., Gomes, E.R., Greene, K.S., Pereira, H.M., Garratt, R.C., Dias, S.M., and Ambrosio, A.L. (2012) Mitochondrial localization and structure-based phosphate activation mechanism of Glutaminase C with implications for cancer metabolism. *Proc. Natl. Acad. Sci. USA* **109**, 1092–1097

6. Robinson, M.M., McBryant, S.J., Tsukamoto, T., Rojas, C., Ferraris, D.V., Hamilton, S.K., Hansen, J.C., and Curthoys, N.P. (2007) Novel mechanism of inhibition of rat kidney-type glutaminase by bis-2-(5-phenylacetamido-1,2,4-thiadiazol-2-yl)ethyl sulfide (BPTES). *Biochem. J.* **406**, 407–414

7. DeLaBarre, B., Gross, S., Fang, C., Gao, Y., Jha, A., Jiang, F., Song, J.J., Wei, W., and Hurov, J.B. (2011) Full-length human glutaminase in complex with an allosteric inhibitor. *Biochemistry* **50**, 10764–10770

8. Thangavelu, K., Pan, C.Q., Karlberg, T., Balaji, G., Uttamchandani, M., Suresh, V., Schüler, H., Low, B.C., and Sivaraman, J. (2012) Structural basis for the allosteric inhibitory mechanism of human

Downloaded from http://www.jbc.org/ at FAPESP - Brazil Consortia on August 12, 2013

kidney-type glutaminase (KGA) and its regulation by Raf-Mek-Erk signaling in cancer cell metabolism. *Proc. Natl. Acad. Sci. USA* **109**, 7705–7710

9. Katt, W.P., Ramachandran, S., Erickson, J.W., and Cerione, R.A. (2012) Dibenzophenanthridines as inhibitors of Glutaminase C and cancer cell proliferation. *Mol. Cancer. Ther.* **11**, 1269–1278

10. Vander Heiden, M.G. (2011) Targeting cancer metabolism: a therapeutic window opens. *Nat. Rev. Drug. Discov.* **10**, 671–684

11. Jones, N.P., and Schulze, A. (2012) Targeting cancer metabolism – aiming at a tumour's sweet-spot. *Drug Discov. Today* **17**, 232–241

12. Kenny, J., Bao, Y., Hamm, B., Taylor, L., Toth, A., Wagers, B., and Curthoys, N.P. (2003) Bacterial expression, purification, and characterization of rat kidney-type mitochondrial glutaminase. *Protein Expres. Purif.* **31**, 140–148

13. Choudhary, C., Kumar, C., Gnad, F., Nielsen, M.L., Rehman, M., Walther, T.C., Olsen, J.V., and Mann, M. (2009) Lysine acetylation targets proteins complexes and co-regulates major cellular functions. *Science* **325**, 834-840

14. Leslie, A.G. (1992) Recent changes to the MOSFLM package for processing film and image plate data. *Joint CCP4 + ESF-EAMCB Newsletter on Protein Crystallography*, **26**, 27–33

15. Evans, P.R. (2005) Scaling and assessment of data quality. *Acta Cryst. Section D* **62**, 72–82

16. McCoy, A.J., Grosse-Kunstleve, R.W., Adams, P.D., Winn, M.D., Storoni, L.C., and Read, R.J. (2007) Phaser Crystallographic software. *J. Appl. Cryst.* **40**, 658–674

17. Adams, P.D., Afonine, P.V., Bunkóczi, G., Chen, V.B., Davis, I.W., Echols, N., Headd, J.J., Hung, L.W., Kapral, G.J., Grosse-Kunstleve, R.W., McCoy, A.J., Moriarty, N.W., Oeffner, R., Read, R.J., Richardson, D.C., Richardson, J.S., Terwilliger, T.C., and Zwart, P.H. (2010) PHENIX: a comprehensive Python-based system for macromolecular structure solution. *Acta Cryst. Section D* ***66,*** 213–221

18. Emsley, P., Lohkamp, B., Scott, W.G., and Cowtan, K.P. (2010) Features and development of Coot. *Acta Cryst. Section D* **66**, 486–501

19. Chen, V.B., Arendall, W.B. 3rd, Headd, J.J., Keedy, D.A., Immormino, R.M., Kapral, G.J., Murray, L.W., Richardson, J.S., and Richardson, D.C. (2010) MolProbity: all-atom structure validation for macromolecular crystallography. *Acta Cryst. Section D* **66**, 12–21

20. Aragão, A.Z., Nogueira, M.L., Granato, D.C., Simabuco, F.M., Honorato, R.V., Hoffman, Z., Yokoo, S., Laurindo, F.R., Squina, F.M., Zeri, A.C., Oliveira, P.S., Sherman, N.E., and Paes Leme, A.F. (2012) Identification of novel interaction between ADAM17 (a disintegrin and metalloprotease 17) and thioredoxin-1. *J. Biol. Chem.* **287**, 43071–43082.

21. Yuneva, M.O., Fan, T.W., Allen, T.D., Higashi, R.M., Ferraris, D.V., Tsukamoto, T., Matés, J.M., Alonso, F.J., Wang, C., Seo, Y., Chen, X., and Bishop, J.M. (2012) The metabolic profile of tumors depends on both the responsible genetic lesion and tissue type. *Cell Metab.* **15**, 157–170

22. Campos-Sandoval, J.A., López de la Oliva, A.R., Lobo, C., Segura, J.A., Matés, J.M., Alonso, F.J., and Márquez, J. (2007) Expression of functional human glutaminase in baculovirus system: affinity purification, kinetic and molecular characterization. *Int J Biochem Cell Biol* **34**, 765–773

Downloaded from http://www.jbc.org/ at FAPESP - Brazil Consortia on August 12, 2013

23. Gorman, M.W., He, M.X., Hal, C.S., and Sparks, H.V. (1997) Inorganic phosphate as regulator of adenosine formation in isolated guinea pig hearts. *Am J Physiol* **272**, H913–H920

24. Read, R.J., and Schierbeek, A.J. (1988) A phased translation function. J. Appl. Cryst. 21, 490–495.

25. Van Heel, M., Portugal, R., Rohou, A., Linnemayr, C., Bebeacua, C., Schmidt, R., Grant, T.R., and Schatz, M. (2012) Four-Dimensional Cryo Electron Microscopy at Quasi Atomic Resolution: IMAGIC 4D in International Tables for Crystallography Volume F: Crystallography of biological macromolecules (Second Edition) Editors: E. Arnold, D. M. Himmel and M. G. Rossmann, pp. 624–628

26. Godfrey, S.S., Kuhlenschmidt, T., Curthoys, N.P. (1977) Correlation between activation and dimer formation of rat renal phosphate dependent glutaminase. *J. Biol. Chem.* **252**, 1927–1931

27. Morehouse, R.F., and Curthoys, N.P. (1981) Properties of rat renal phosphate-dependent glutaminase coupled to Sepharose. Evidence that dimerization is essential for activation. *Biochem. J.* **193**, 709–716

28. Olsen, B.R., Svenneby, G., Kvamme, E., Tveit, B., and Eskeland, T. (1970) Formation and ultrastructure of enzymically active polymers of pig renal glutaminase. *J. Mol. Biol.* **52**, 239–245

29. Olsen, B.R., Torgner, I.A., Christensen, T.B., and Kvamme, E. (1973) Ultrastructure of pig renal glutaminase. Evidence for conformational changes during polymer formation. *J. Mol. Biol.* **74**, 239–251

30. Curthoys, N.P., Kuhlenschmidt, T., and Godfrey, S.S. (1976) Regulation of renal ammoniagenesis, purification and characterization of phosphate-dependent glutaminase from rat kidney. *Arch. Biochem. Biophys.* **174**, 82–89

31. Josephs, R., and Borisy, G. (1972) Self-assembly of glutamic dehydrogenase into ordered superstructures: multichain tubes formed by association of single molecules. *J. Mol. Biol.* **65**, 127–155

32. Curthoys, N.P., and Watford, M. (1995) Regulation of glutaminase activity and glutamine metabolism. *Annu. Rev. Nutr.* **15**, 133–159

33. Fan, T.W., Higashim, R.M., and Macdonald, J.M. (1991) Emergence and recovery response of phosphate metabolites and intracellular pH in intact Mytilus edulis as examined in situ by in vivo 31P-NMR. *Biochim. Biophys. Acta* **1092**, 39–47

ACKNOWLEDGEMENTS

We thank LNBio, for financial support and access to itsfacilities (LPP, LEC, MAS, LBE, LVV and Robolab); LNNano for access to LME; and LNLS, for access to D03B-MX1 beamline. We thank Dr. Alessandra Girasole for secretarial and technical support of Annelize Aragão and Romênia Domingues for helping with the MS analysis. We thank Dr. Richard C. Garratt (IFSC, USP) for critical reading of the manuscript. The atomic coordinates and structure factor have been deposited in the Protein Data Bank under code 4jkt (BPTES-bound GAC).

FOOTNOTES

*This work was supported by FAPESP under grants 2009/10875-9 (SMGD), 2010/05003-0 and 2012/14298-9 (ALBA), and fellowships 2010/05987-0 (APSF), 2010/05987-0 (AC), 2011/06654-7 (KAG) and 2009/54067-3 (AFPL).

FIGURE LEGENDS

Downloaded from http://www.jbc.org/ at FAPESP - Brazil Consortia on August 12, 2013

FIGURE 1. *GAC polymerization is essential for enzymatic activation.* (A) Size-exclusion chromatography analysis of serial dilutions for wild type and mutated GAC in the presence or absence of 20 mM phosphate. The green region delimits the expected Stokes radii between GAC dimers, D, and tetramers, T, calculated based on the crystal structure (3ss3) dimensions. The light purple region delimited by V in the GAC. K325A graph indicates the void volume of the gel-filtration column used. Asterisk indicates a previously published result for wild-type GAC (5). (B) The software DigitalMicrograph (Gatan, USA), was used to estimate the two orthogonal size distributions (short and long dimensions) of the wild-type and point-mutant glutaminase particles, formed under the diverse conditions described in the main text (absence or presence of 20 mM phosphate and cross-linked vs. non-cross-linked particles). (C) Supra-tetrameric organization of GAC upon the addition of 20 mM phosphate, a well-known activator of GLS1 glutaminases. (D) Box plot and scatter representation of the two orthogonal dimensions for GAC wild-type and point mutants, as taken from the TEM micrographs. (E) Chemically crosslinked GAC super-oligomers. Some of the observed filaments resemble lateral association between two simple filaments. (F) GAC.K325A presents a much higher catalytic efficiency, already in the absence of phosphate, when compared to wild-type GAC and the inactive GAC.R322A. (G) The high enzymatic efficiency of GAC.K325A correlates well with its tendency to self-assemble into rod-like polymers, regardless of the presence of the activator inorganic phosphate (left box) and DSS. Conversely, the catalytically inactive GAC.R322A protein, remains in its tetrameric form, even in the presence of 20 mM phosphate (right box). Scale bars represent 100 nm.

FIGURE 2. *Glutaminase isozymes versus self-assembly tendency.* TEM analysis of the three glutaminase isozymes, crosslinked after incubation with 20 mM phosphate. The average length of the superstructure correlates positively with the previously published glutaminase activity levels (5). GAC is the most active isozyme and forms the longest polymers (top left box), followed by KGA (top right box), with lower activity and shorter structures, and lastly LGA, which is insensitive to phosphate, and, accordingly, does not form filaments (bottom left box). Unless otherwise specified, scale bars represent 100 nm.

FIGURE 3. *BTPES inhibits GAC super-structure formation.* (A) Dose-response profile of BPTES inhibition on GAC, assayed in the presence of 20 mM phosphate, showing two complementary effects on the apparent turnover rates and the Michaelis constant of the enzyme. (B) BPTES traps the gating loop (black ribbons) in a rigid open conformation relative to the catalytic pocket of GAC (delimited by a green surface). (C) Stereographic view of a Fourier $2F_{obs}$-F_{calc} map (at 1σ) confirming the proposed conformation in the refined crystallographic model. (D) TEM analysis of the effects of BPTES on the formation of GAC superstructure. The filament formation is hindered regardless of whether BPTES is added to the protein solution prior to (middle box) or after (lower box) incubation with 20 mM phosphate. Conversely, GAC.K325A is catalytically insensitive to BPTES treatment (E), and this inhibitor is also incapable of disrupting the non-crosslinked GAC.K325A filaments (F).

FIGURE 4. *A model of GAC super-oligomer assembly.* (A) The removal of high frequencies (strongly associated with noise) from the TEM micrographs highlights the right-handed double-strand nature of the superstructure allowing the determination of its geometric features. (B) Cross-linked MS/MS spectra were manually validated for b and y ion series of the α and β chains of cross-linked peptides (between residues Lys181 and Lys207, Lys202 and Lys578 and Lys403 and Lys512. The ions are indicated by arrows with corresponding m/z value. (C) Relative position of DSS-linked lysine pairs in the tetramer, as identified by MS. The boundaries of the active sites are delimited by solid surfaces. †Lys578 is not modeled in the crystal structure. The proposed single strand growth direction across the longest axis of the tetramer, via an end-to-end interaction between pairs of N-terminal domains. Alternating orange and yellow colors facilitate the identification of the tetramers along the single strand. (D) One lysine residue from each cross-linked pair was individually substituted by a glutamate and assayed for enzymatic activity (left box) and superstructure formation (right box). The N-terminal region mutants (GAC.K202E and GAC.K207E) enhanced both effects. On the other hand, GAC.K512E, within the glutaminase domain, generated a non-functional protein, similarly to the acetylation mimetic GAC.K316Q. The green region delimits the

Downloaded from http://www.jbc.org/ at FAPESP - Brazil Consortia on August 12, 2013

expected Stokes radii between GAC dimers, D, and tetramers, T, calculated based on the crystal structure dimensions. The asterisk indicates a previously published result for wild-type GAC (5). (E) The double strand was manually modeled (i), using two entwined copies of the single strand from (C) and following the geometric restrictions of (A). (ii) The calculated Fourier F_{calc} map (with amplitudes and phases from the double strand model) - limited to 35 Å maximum resolution – was two-dimensionally projected and the end result is shown in (iii). All features are comparable to those observed in (iv), concerning the presence of alternating high-density narrow regions (indicated by full triangles), and low-density broad, disc-like regions (indicated by void triangles).

FIGURE 5. *GAC superstructure in cell models.* (A and B) Endogenous and V5-tagged ectopic proteins expressed to similar levels. A stable MDA-MB 231 clone selected after GAC.K325A-V5 transfection presented larger and more heterogeneous cell area (C), proliferated more (D), and consumed more glutamine from the culture media (E), all compared to cells bearing the V5-tagged wild type protein or a mock plasmid. (F) Relative mRNA levels of ASCT2 and SN2 glutamine transporters, as defined by quantitative PCR using the rRNA 18S as a house-keeping gene, showing that the GAC.K325A-V5 cells do not over-express these transporters. (G) Glutaminase activity from whole-cell lysate, in the presence of 20 mM phosphate, showing consistently higher turnover rates for the GAC.K325A-V5 samples, against the physiological glutamine levels in tumors. (H) Left panel: Step Gradient SDS-PAGE (3-15%) followed by immunoblotting of UV-induced crosslinked intracellular protein with incorporated photo-reactive amino acids, showing the tendency of the GAC.K325A-V5 to form higher molecular weight superstructures within the cells. The UV-induced cross-linking was performed in living, intact cells in culture. Right panel: Densitometry was performed in conditions of non-saturated signal, using ImageJ (http://rsb.info.nih.gov/ij/), to evidence the differential cross-linking of bigger species for GAC.K325A-V5. (I) Similarly to what was observed for the recombinant protein, cells expressing the fiber-prone hyper-active GAC.K325 mutant (GAC.K325A-V5) were less sensitive to BPTES treatment, still proliferating more (left box) and consuming more glutamine (right box) than BPTES-treated counterparts. (J) The knocking-down of endogenous GAC favored the enhancing of the phenotypic differences observed above, better highlighting the outcome from GAC.K325A-V5 expression.

Downloaded from http://www.jbc.org/ at FAPESP - Brazil Consortia on August 12, 2013

TABLE 1

X-ray crystallography data collection parameters and structure refinement statistics.

BPTES-bound mouse Glutaminase C (PDBIB 4jkt)			
Data Collection		Model Refinement	
Beamline	D03B-MX1 at LNLS, Brazil	Resolution range (Å)	20.0 – 2.77
Wavelength (Å)	1.608	Reflections (cross-validation)	63892 (5952)
Space group	$P2_12_12_1$	R_{factor}/R_{free} (%)	25.3 / 29.5
Cell parameters a, b, c (Å)	100.7, 140.2, 180.9	Average B-factor (Å^2)	
Resolution range (Å)	38.4 - 2.77 (2.82 - 2.77)	main chain (no. of residues)	32.9 / 3.4 (1563)
Unique reflections	63967 (2039)	side chain (no. of residues)	32.8 / 4.3 (1362)
Multiplicity	3.3 (2.6)	BPTES (no. of molecules)	44.1 / 9.2 (2)
$R_{p.i.m.}$ (%)	11.0 (24.0)	solvent (no. of molecules)	24.4 / 5.9 (265)
Completeness (%)	95.5 (46.2)	R.m.s.d. from standard geometry	
<I/σ(I)>	4.5 (2.8)	bond length (Å)	0.003
Average mosaicity (°)	1.0	bond angles (°)	0.783
B-factor Wilson Plot (Å^2)	40.5	Ramachandran plot	
Monomers/AU	4	most favored (%)	94.5
Solvent content (%)	59.2	allowed (%)	4.8
Matthews coeff. (A^3/Da)	3.01	outlier (%)	0.7

Data for outer shell shown in parentheses.

Downloaded from http://www.jbc.org/ at FAPESP - Brazil Consortia on August 12, 2013

FIGURE 1

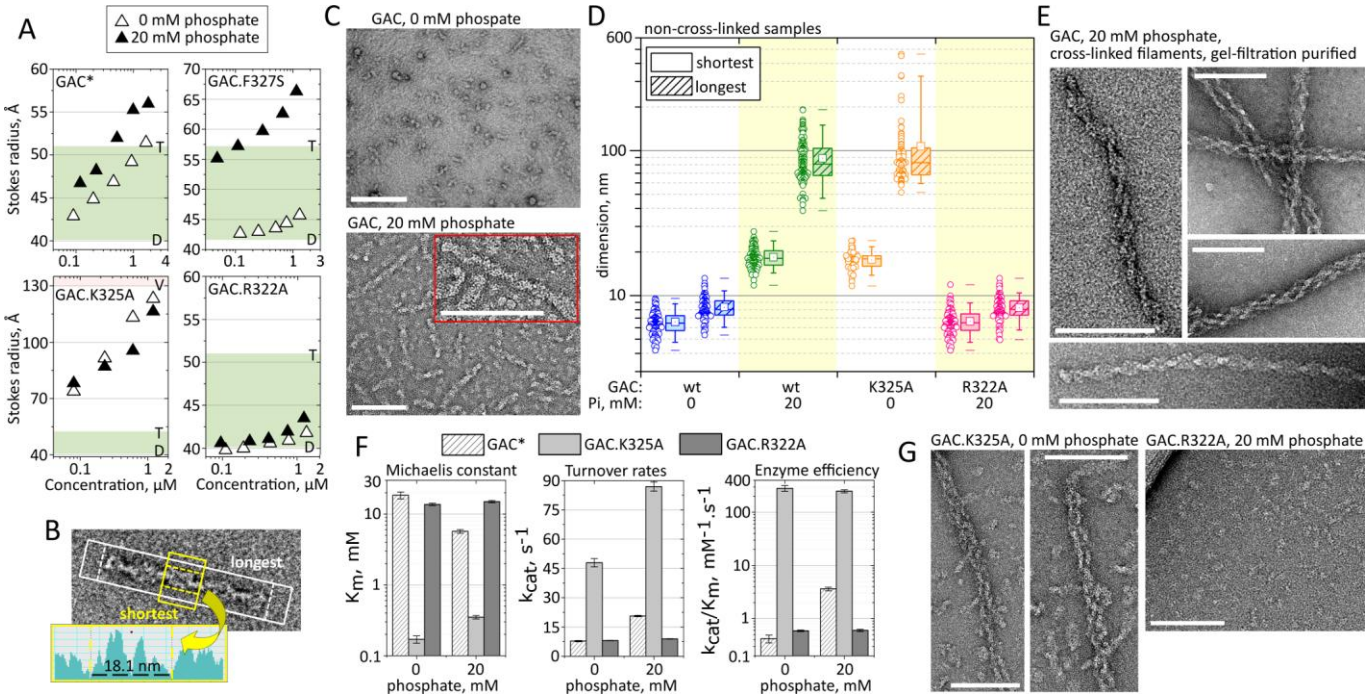

Downloaded from http://www.jbc.org/ at FAPESP - Brazil Consortia on August 12, 2013

FIGURE 2

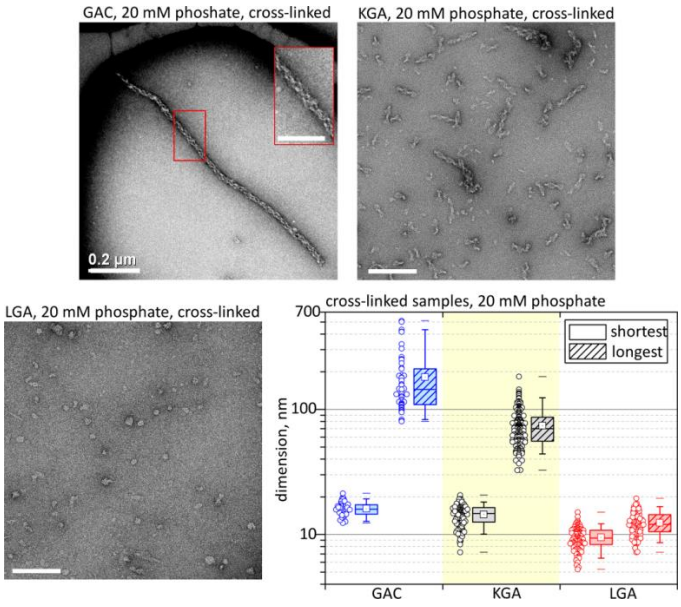

Downloaded from http://www.jbc.org/ at FAPESP - Brazil Consortia on August 12, 2013

FIGURE 3

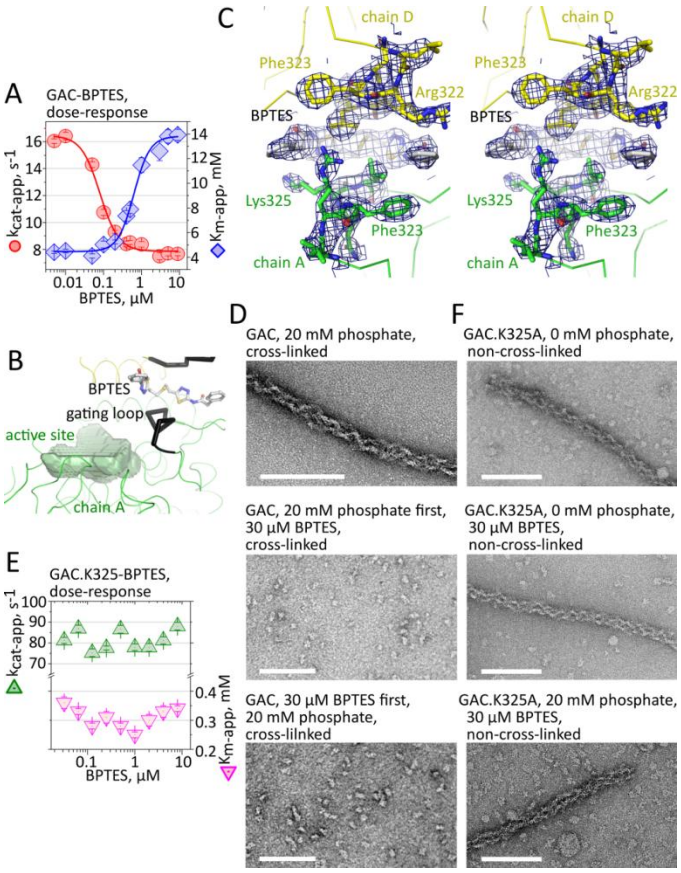

Downloaded from http://www.jbc.org/ at FAPESP - Brazil Consortia on August 12, 2013

FIGURE 4

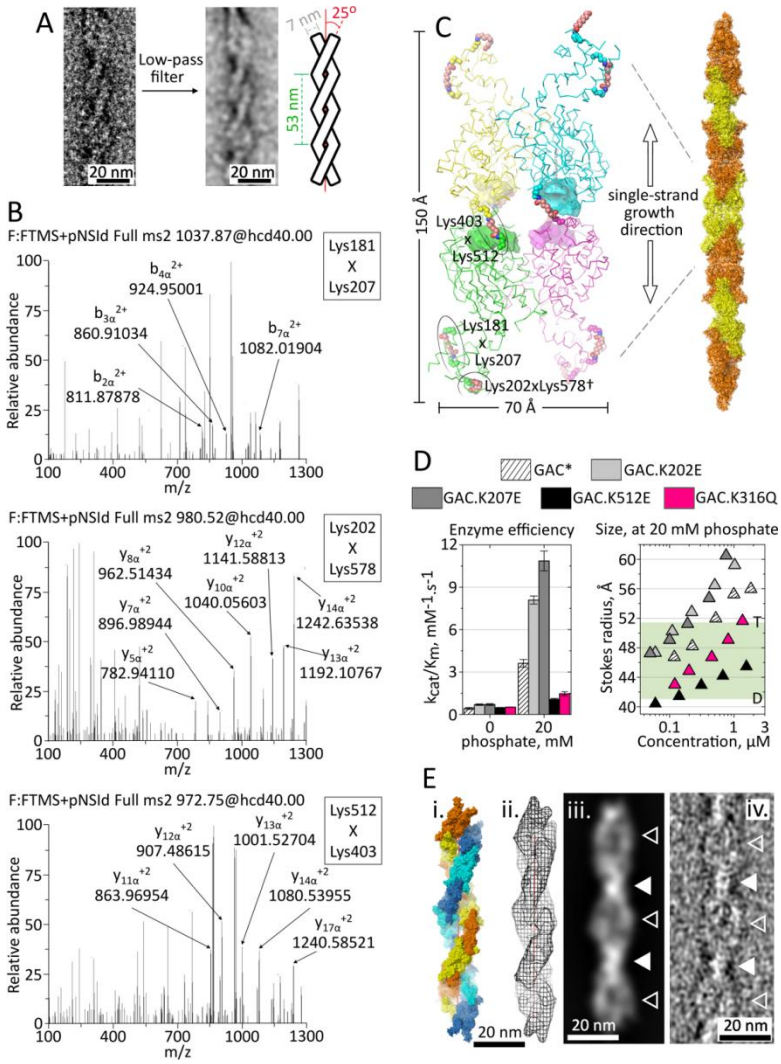

Downloaded from http://www.jbc.org/ at FAPESP - Brazil Consortia on August 12, 2013

FIGURE 5

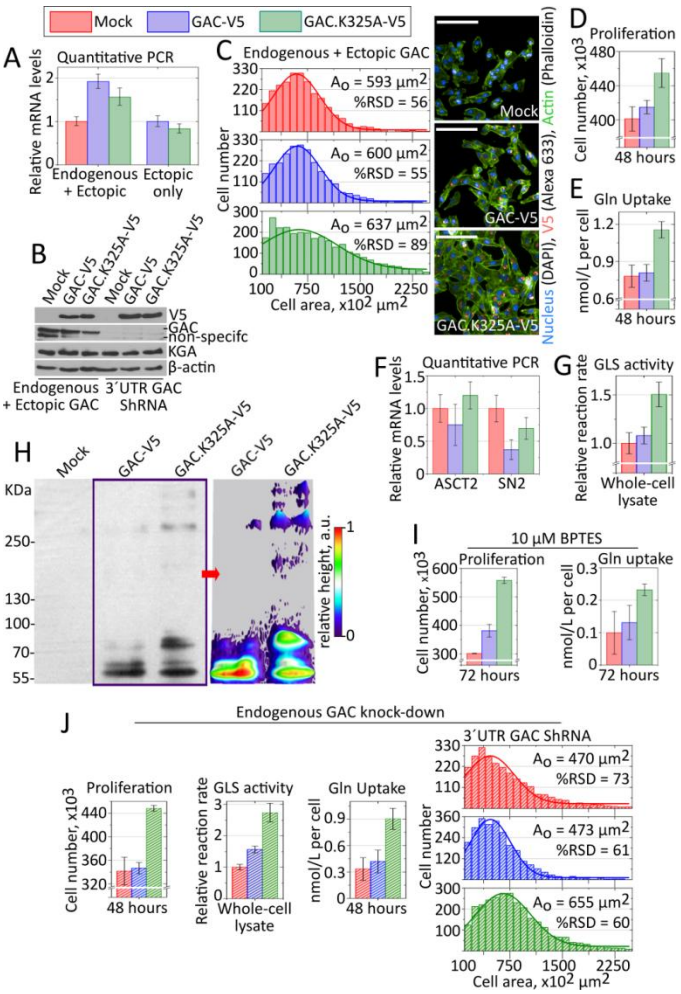

Downloaded from http://www.jbc.org/ at FAPESP - Brazil Consortia on August 12, 2013